Article:
Sarhosis, V orcid.org/0000-0002-8604-8659, Forgács, T and Lemos, JV (2019) A discrete approach for modelling backfill material in masonry arch bridges. Computers and Structures, 224. 106108. ISSN 0045-7949

https://doi.org/10.1016/j.compstruc.2019.106108

A discrete approach for modelling backfill material in masonry arch bridges

Vasilis Sarhosis[1*], Tamás Forgács[2], Jose V. Lemos[3]

[1]School of Civil Engineering, University of Leeds, Leeds, LS2 9JT, UK
[2] University of Technology and Economics, H-1111 Budapest, Műegyetem rakpart 3.
[3]National Laboratory for Civil Engineering (LNEC), Lisbon, Portugal

Abstract

Masonry arch bridges form a significant portion of the European transport infrastructure network. Many of these bridges are relatively old but still in service. Increasing vehicle loads and speeds have highlighted the need for reliable estimates of their service condition. Past research demonstrated that load-carrying capacity of a masonry arch bridge is a function of the soil response. However, today, the approaches used for the simulation of soil in masonry arch bridges are over-simplistic and most of them do not take into account the soil-structure interaction phenomena. This paper presents a novel modelling approach, based on the discrete element method, for the simulation of backfill material in masonry arch bridges. According to the method, bricks in the barrel vault are simulated as an assembly of distinct blocks separated by zero thickness interfaces at each mortar joint. Backfill is represented as an assemblage of densely packed discrete irregular deformable particles, here called "inner-backfill particles". A series of computational models were developed and their results are compared against full-scale experimental test results. A good agreement between the experimental and the numerical results was obtained which demonstrates the huge potential of this novel modelling approach. One of the major advantages of the proposed approach is its ability to simulate the initiation and propagation of cracking in the backfill and arch ring with the application of the external load. It is envisaged that the current modelling approach can be used by bridge assessment engineers for understanding soil pressures and load distribution on the backfill and arch ring and thus develop serviceability criteria for masonry arch bridges of their care.

Keywords: masonry, backfill, interface elements, discrete element modelling, arches, bridges

Highlights

- A novel approach to represent cracking in backfill of masonry arch bridges proposed
- Backfill is considered as an assemblage of densely packed discrete irregular particles
- A fair to good agreement between the experimental and the numerical results was obtained
- Initiation and propagation of cracking in soil is captured with the application of external load
- The approach can be used to better understand the load distribution in masonry arch bridges

*__Corresponding author:__ Dr Vasilis Sarhosis, School of Civil Engineering, University of Leeds, LS2 9JT, Leeds, UK, email: v.sarhosis@leeds.ac.uk

1 Introduction

Masonry arch bridges form an integral part of the European railway and highway bridge stock. Although most of the masonry arch bridges were constructed back in the 19th century, such structures are still standing and carrying today's traffic loads. Weathering, demands of increasing load intensity and axle loads, as well as factors such as increased frequency of flood events brought about by climate change have introduced a poorly constrained uncertainty on the long term performance of such infrastructure assets. The cost of replacing masonry infrastructure in the UK alone would run into tens of billions of pounds, and their aesthetic and heritage value is significant (e.g. the Grade II-listed Hungerford Canal Bridge, in Berkshire, England). Moreover, failure of such infrastructure could lead to significant direct and indirect costs to the economy and society and could hamper rescue and recovery efforts. Therefore, there is a pressing need to accurately assess the performance of ageing masonry infrastructure and provide detailed and accurate data that will better inform maintenance programmes and asset management decisions. Without a strategic approach to caring for our ageing masonry infrastructure, we run the risk of over-investing in some areas while neglecting others that are in need of our attention, or indeed risk failing to address economic and societal need.

Over the last thirty years, a significant amount of experimental work has been carried out in order to understand the effect of backfill into the serviceability and ultimate load bearing capacity of masonry arch bridges. In a series of tests to destruction, Davey [1] found that soil-structure interaction increased the load bearing capacity of a masonry arch bridges and therefore such effects should not be ignored when evaluating the strength of a masonry arch bridge. Later, experimental testing with a view to underspend the soil-structure interaction have been carried out by Harvey et al. [2] and Melbourne et al. [3]. In Harvey's tests, soil pressures were relatively low, which according to [4], this might be due to the interface of the retaining walls which were built close behind the springing. In contrary, experimental tests carried out by Melbourne and Walker [5] revealed the development of relatively high soil pressure, even though pressure distribution was not recorded during testing. Moreover, with a view to investigate the distribution of the external load applied on an arch bridge, Fairfield [6] carried out several tests on semi-circular and segmental model arches with voussoirs made of timber. The backfill was uniformly graded dry sand and restrained by two glass walls. From the results analysis it was found that the collapse load increases with increased fill depth. Moreover, Hughes [7] constructed 1/6 scale models of a prototype masonry arch bridge containing backfill and carried out a series of centrifuge tests on it. They found that changing the fill type had a significant effect on the load bearing capacity. Similar observation about the effect of the backfill into the load carrying capacity of a masonry arch bridge have been observed by Gilbert et al. [8]. By testing a series of small-scale arch bridges with different fill materials, it was found that the load carrying capacity of masonry arch bridges with limestone as backfill is double compared to the one with clay backfill material. One the other hand, a significant number of experimental tests have been carried out on full-scale masonry arch bridges. For example, Melbourne et al. [9] performed a full-scale model test on a 6 m span multi-ring brickwork arch bridge in the TRRL Laboratory to identify the effect of the spandrel walls and the backfill material. Test results showed that failure was due to a four-hinge mechanism accompanied with ring separation. Also, it was observed that the backfill provided a significant lateral restraint to the deformation of the arch ring.

Significant efforts have also been made towards the development of analytical and advanced computational methods of analysis for masonry arch bridges. Experience from such studies demonstrated that the structural assessment of masonry arch bridges is complex and requires the development of advanced numerical models of analysis that consider the geometric non-linearity between masonry units and account for the interaction between the arch ring, parapets and fill material. Today, the numerical techniques used for the assessment of masonry arch bridges can be grouped into those based on the macro-modelling approach in which masonry is considered as an anisotropic continuum and the micro/meso-modelling approach which considers masonry as an assemblage of masonry units connected together by mortar joints (such as mathematical programming techniques based on the limit analysis; the finite element method based on contact element; and the discrete element method [10]). Numerical methods of analysis, like the Finite Element Method (FEM) based on the macro-modelling approach (Lourenco [11]), have been applied to understand the three-dimensional

behaviour of masonry structures. However, in such cases, the description of the discontinuity which characterises ageing masonry infrastructure is limited since they consider masonry as an anisotropic continuum (Boothby [12]). Recent advances in the mathematical programming techniques based on limit analysis [13-17] highlighted that they are quick to construct the model and obtain the results. However, a limitation of the approach is that only the ultimate load bearing capacity and the corresponding failure mode can be determined. Moreover, the backfill is replaced with external loads on the extrados of the barrel, while the passive earth pressure was considered with non-linear spring elements [37]. On the other hand, the finite element models can implement complex material constitutive laws to consider the heterogeneous and anisotropic behaviour of masonry [18, 19]. Nevertheless, the description of discontinuity (e.g. voussoir to voussoir, voussoir to backfill) is difficult since they tend to consider masonry as a continuous material [19, 20]. Contrarily, the interaction of distinct blocks can be easily modelled in discrete element methods in which masonry can be considered as an assemblage of masonry units bonded together by zero thickness interfaces, which can open, close and slide according to stresses applied to them (Forgács et al. [21]; Sarhosis et al. [22]; Forgács et al. [23]). For an extensive discussion on the available experimental and numerical approaches for masonry arch bridges, the reader is directed to [24] and [25]. From the above, the presence of backfill has a significant influence on the behaviour of a masonry arch bridge. According to [13] & [26], for a numerical model to accurately predict the effects of backfill, it is essential that the model allows for:

i) distribution of concentrated loads applied on the top surface of the bridge through the backfill of the barrel arch ring;
ii) dead load of the backfill material so that the voussoirs of the arch ring are in compression; and
iii) passive earth resistance i.e. restrain sway of the barrel arch ring by generating passive resistance pressure and prevention of destabilising effects of the bridge due to variable live loads.

However, the quantification of the passive soil pressure is not a straightforward task. The classical approaches adopted for estimating passive soil pressure in soils cannot be directly used for the analysis of masonry arch bridges. This is because full passive pressures are not usually mobilised in the backfill, when external loads are applied in the masonry arch bridge. According to Fang et al. [27], the mobilization level will depend on the amount of movement of the barrel and the soil type. Therefore, accurate numerical models need to be developed for being able to model frictional backfill material directly, which will allow one to study the overall behaviour of the system.

In this paper, a novel modelling approach for the simulation of backfill in masonry arch bridges has been proposed. The approach is based on the discrete element method of analysis which was originated from the word developed by Cundall in 1971 [28]. According to the method, bricks in the barrel vault are represented as an assembly of distinct blocks separated by zero thickness interfaces at each mortar joint while backfill is represented as an assemblage of densely packed discrete irregular deformable particles. In this way, the discrete nature of backfill can be represented. In addition, the initiation and propagation of cracks in backfill with the application of external load can be estimated. Since backfill is represented by irregular in shape particles, the mechanical behaviour of the backfill is influenced by the size and properties of the irregular soil particles and their contact properties. A series of computational models were developed and their results are compared against full-scale experimental results. The proposed approach is able to estimate the initiation and propagation of cracking in the backfill and arch ring with the application of the external load. It is envisaged that the current modelling approach can be used by bridge assessment engineers for understanding soil pressures and load distribution on the backfill and arch ring and thus develop serviceability criteria for masonry arch bridges of their care.

2 An alternative approach to simulate the backfill material in masonry arch bridges

The proposed model is based on a phenomenological approach, which aims to simulate both the backfill material and soil-structure interaction phenomena in masonry arch bridges when subjected to external load. The proposed model was developed in a discrete element framework, the two-dimensional code

UDEC [29]. However, the proposed methodology can be adapted to any discrete element software. The key features required to implement the proposed approach are described below.

2.1 Representation of the elements

In the presented DE model, masonry units and the backfill are represented by polygonal blocks that may take any arbitrary geometry. These elements are made deformable by subdivision into finite elements, commonly denoted as zones in DEM codes. Every discrete element is internally discretised into uniform strain simplexes (triangular elements in 2D). Inside every simplex, a linear translation field can be defined with the linear interpolation of the nodal translations. In this way, the unknowns of the model are the displacements at the nodes. Each internal zone responds according to a prescribed linear or non-linear stress-strain law, similarly to continuum elements in the finite element method (FEM).

The discontinuous nature of backfill or soil is represented by a series of irregular in shape particles of polygonal or Voronoi shape (Mayya and Rajam [30]). Such fictitious irregular particles, here named "inner-backfill particles" are shown in Figure 1. Inner-backfill particles are also subdivided into simple triangular finite elements (**Error! Reference source not found.**), which give a detailed approximation of the strain field. These particles containing internal meshing can be either assumed to behave in an elastic or in an elasto-plastic manner. The appropriateness of each of these two assumptions to model backfill will be examined below. Also, the size and shape of the irregular inner-backfill particles will be investigated too, as these parameters will affect the mechanical behaviour of the backfill.

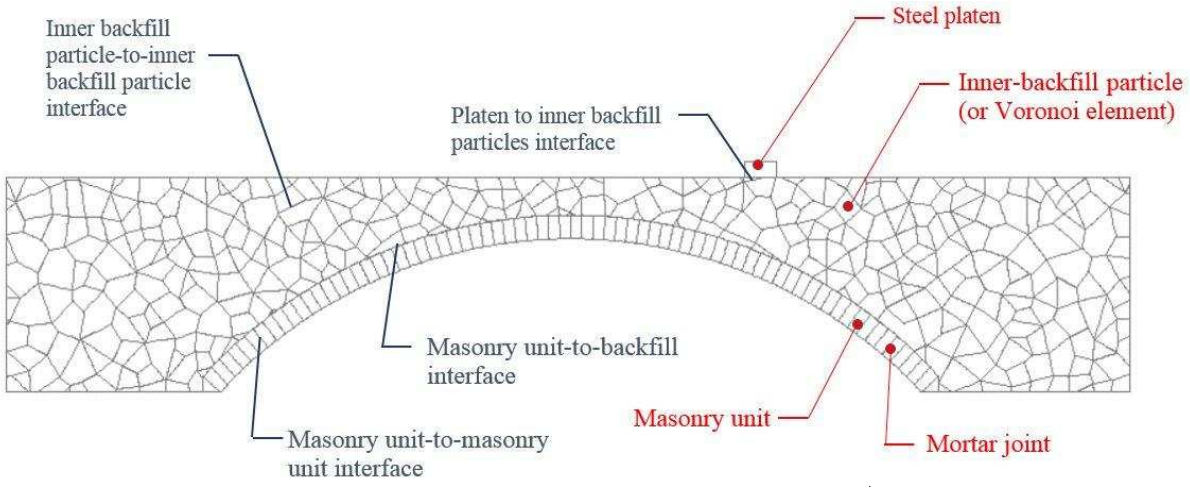

Figure 1 - Representation of backfill in a masonry arch as a series of polygonal particles herein called *"inner-backfill particles"*

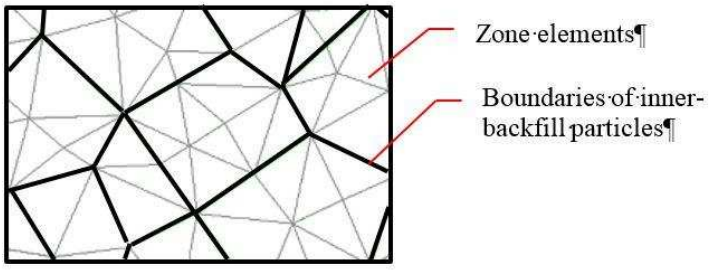

Figure 2 - Triangular zones in the "inner-backfill particles"

2.2 Contact representation

The discrete elements can interact with each other through zero-thickness interface elements. These interfaces can be viewed as locations where mechanical interactions between the blocks takes place and

their behaviour are governed by appropriate stress-displacement constitutive laws. These places could be potential fracture slip lines as well. This approach is similar to the 'simplified micro-modelling' option in finite element models of masonry [11]. However, the numerical treatment is different in DEM. At the interfaces, blocks (e.g. inner-backfill particles, masonry units, steel platen etc) are connected kinematically to each other by sets of point contacts, along the outside perimeter of the blocks, at locations where corners or edges meet [31]. The main advantages of the point-contact hypothesis method are its generality and its simplicity at being able to handle the various types of geometric interaction between the blocks. It can also consider large block movements, including cases of detachment and re-closure when external forces are applied to them, with no attempt to obtain a continuous stress distribution through the contact surface.

In the proposed numerical approach, there are four different types of interfaces. These are shown in Figure 1 and include:

a) Masonry unit to masonry unit interface;

b) Masonry unit to backfill interface;

c) Inner-backfill particles to inner backfill particles; and

d) Soil platen to inner-backfill particle interface.

In the code UDEC, blocks are characterised by rounded edges instead of sharp corners. Rounding affects only the detection and geometrical characterisation of the contacts between the blocks. Contact between sharp corners in blocks is difficult to treat numerically, and may lead to corner interlocking under large displacements. Block and zone geometries and properties are not affected by rounding. The rounding length can be defined by the user (default value is 0.5) and recommended to be at least 1% of the of the representative block edge length in the model. The rounding is determined by a termed called “rounding length” which gives the distance between the corner and between the point on the edge where the rounding arch touches the edge (Figure 3e) and is the same for all the blocks in a model. Rounding affects only the recognition and geometrical characteristics of contacts. Other characteristics such as the estimation of the stains in a block are based on the original geometry without rounding. The nodes have two translational degrees of freedom. The displacement vector of node, n, consists of two scalar components:

$$\boldsymbol{u}(t) = \begin{bmatrix} u_x^n(t) \\ u_y^n(t) \end{bmatrix} \tag{1}$$

And these are collected into the total displacement vector of the system containing altogether N nodes:

$$\boldsymbol{u}^n(t) = \begin{bmatrix} u^1(t) \\ u^2(t) \\ \cdot \\ \cdot \\ \cdot \\ \cdot \\ u^N(t) \end{bmatrix} \tag{2}$$

Figure 3 shows the mechanical representation of the interfaces between adjacent blocks. From Figure 3a, for each contact point, there are two spring connections. These can transfer either a normal force or a shear force from one block to the other (Figure 3b&c). The normal and the shear direction in case of a corner-to-corner and a corner-to-edge contacts are explained in Figure 3d&e, respectively. In the normal direction, the mechanical behaviour of the joints (i.e. the zero-thickness contact interface) is governed by the following equation:

$$\Delta\sigma_n = k_n \ \Delta u_n \quad (3)$$

where k_n is the normal stiffness of the contact and Δu_n is the increment in normal contact displacement, i.e., the relative displacement between the blocks at the contact point. Similarly, in the shear direction, the mechanical behaviour is controlled by the constant shear stiffness k_s using the following expression:

$$\Delta\tau_s = k_s \ \Delta u_s \quad (4)$$

where $\Delta\tau_s$ is the change in shear stress, and Δu_s is the increment in shear displacement. There is no integration of stresses on the contact surface as in FEM joint elements (Sarhosis [32]). However, an area is assigned to each contact point, and all the areas add up to the total contact surface. Therefore, contact stresses can be evaluated at each point contact, and the standard joint constitutive models, relating normal and shear stresses with contact displacements, can be employed.

In the present research work, the contacts are assumed to follow the Mohr-Coulomb failure criterion, commonly used to represent shear failure in soils and rocks. The criterion has a limiting tensile strength, f_t. If the contact normal stress exceeds the tensile strength, then the normal stress is set to zero and the interface opens. Alternatively, at those contacts undergoing compression, a small overlap will occur between block edges (Figure 3b). The amount of overlap is controlled by the normal stiffness. Similarly, in shear, in the elastic range, the response is controlled by contact shear stiffness (Figure 3c). In addition, in the shear direction, slippage between blocks occurs when the tangential or shear stress at a contact exceeds a critical value τ_{max} defined by:

$$|\tau_s| \leq c + \sigma_n \tan\varphi = \tau_{max} \quad (5)$$

where $\mu = \tan(\varphi)$ is the friction coefficient and φ the angle of friction and c the cohesive strength. After slip takes place, the shear stress is reduced according to the Mohr-Coulomb criterion, but using residual values for cohesion (c_{res}) and friction (φ_{res}), as shown in Figure 3c. Non-associative flow rule is applied therefore the dilation angle (ψ) is set to zero. After a contact breaks or slips, forces are redistributed and it might cause adjacent contacts to break. During the process, the micro-properties at the inner-block interfaces control the mechanical response of the material and should be calibrated to represent the macro-behaviour. Cracks are initiated at the contact between interfaces. When the stress applied on the contact exceeds either the tensile or the shear strength, inner blocks can separate or slide. In this way, cracking at the brick, mortar and/or brick-to-mortar interface can be represented.

As a block move during the course of the simulation, it is remapped and tested for contact with new neighbours. A triggering neighbourhood search is undertaken. This process is triggered by the accumulated movement of the block. A variable u_{acc}, set to zero after each remap and is updated at every time-step:

$$u_{acc} = u_{acc} + \max\{\text{abs}(du)\} \quad (6)$$

where du is the incremental displacement of a corner, and the max { } function is taken over all corners of the block. When u_{acc} exceeds a quarter of the rounding length, remapping and contact testing is activated. The rounding length is also used to determine whether a contact is created or deleted. If two blocks are found to be separated by a gap that is equal to or less than the rounding length, a contact is created. This logic ensures that the data structure for all contacts is in place before physical contact takes place.

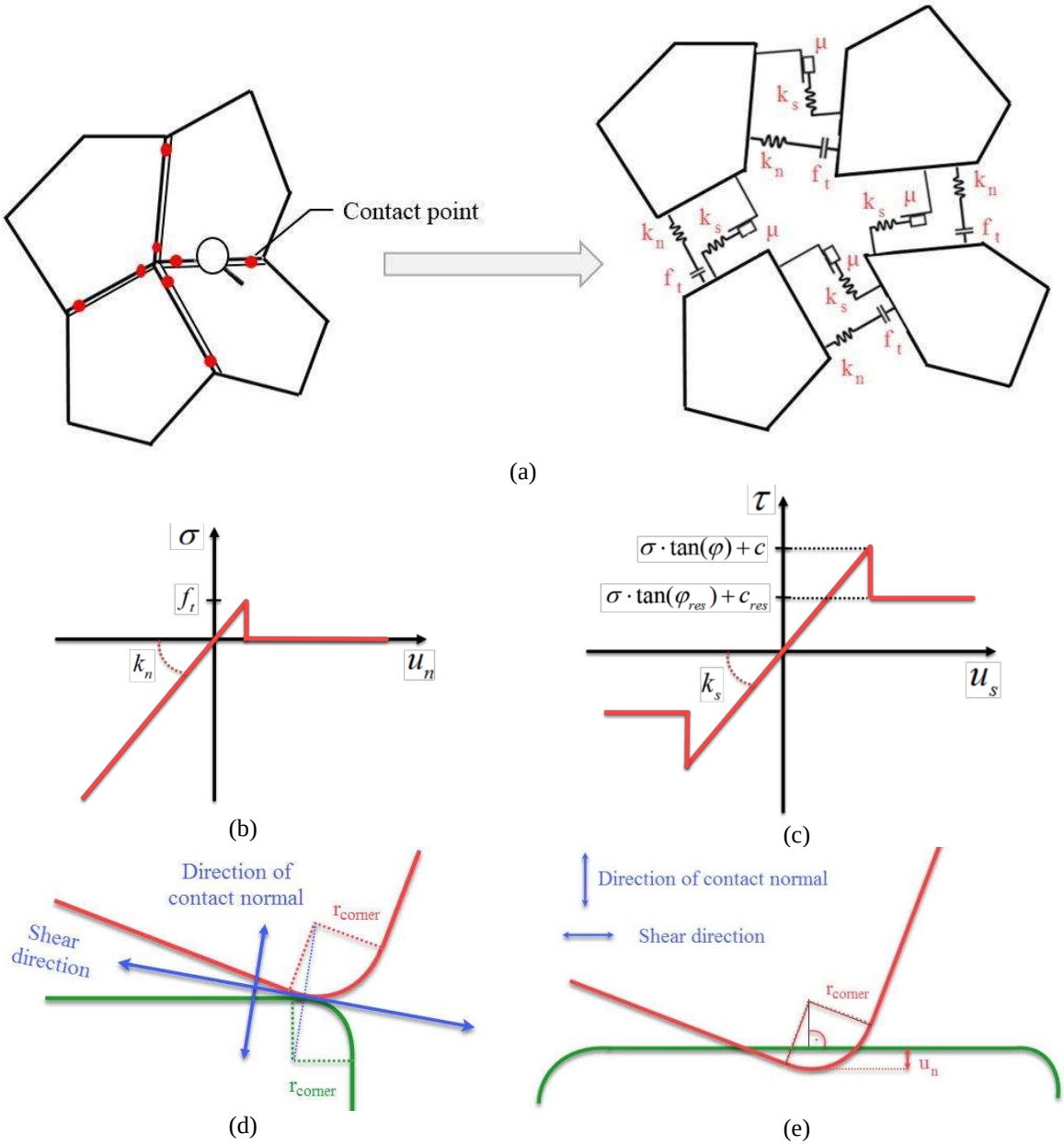

Figure 3. (a) Mechanical representation of the interfaces between adjacent Voronoi elements in the masonry arch bridge shown in Figure 1; (b) behaviour under uniaxial loading; and (c) shear behaviour, Mohr-Coulomb slip model; ; (d) corner-to-corner; (e) corner-to-edge type contact and rounding length representation

2.3 Solution procedure

In the present DEM model, a dynamic solution algorithm is applied. The model unknowns are the displacements at the nodes, which include the block boundary vertices and the internal zone nodes (Figure 2). The equations of motion of the nodes are solved by an explicit time stepping algorithm. The equations of motion for each node are

$$m\frac{d\dot{u}_i}{dt} + \alpha\, m\, \dot{u}_i = f_i, \tag{7}$$

where u_i is the nodal displacement vector of node, (i={x,y}), m is the nodal mass, α is the mass-proportional viscous damping parameter. The nodal force vector is given by a sum of three terms

$$f_i = f_i^c + f_i^e + f_i^a \,, \tag{8}$$

where f_i^c represents the contact forces, for nodes on the block boundaries, f_i^e are the nodal forces obtained from the internal zone stresses, and f_i^a are the external applied loads, including gravity.

The time stepping algorithm employs the central-difference method (e.g. [33]). The finite-difference approximation of equation (4), centred at time t, allows the calculation of the velocity at time (t+Δt/2) as

$$\dot{u}_i^{(t+\frac{\Delta t}{2})} = \left[D_1 \, \dot{u}_i^{(t-\frac{\Delta t}{2})} + \frac{f_i}{m} \Delta t \right] D_2 \,, \tag{9}$$

where $D_1 = (1-\alpha\Delta t/2)$, and $D_2 = 1/(1+\alpha\Delta t/2)$. Then, the new nodal displacements and locations at time ($t+\Delta t$) can be evaluated as

$$u_i^{(t+\Delta t)} = u_i^{(t)} + \dot{u}_i^{(t+\frac{\Delta t}{2})} \Delta t, \tag{10}$$

$$x_i^{(t+\Delta t)} = x_i^{(t)} + \dot{u}_i^{(t+\frac{\Delta t}{2})} \Delta t, \tag{11}$$

The new positions of the block nodes and edges allow the update of the location and orientation of the existing contacts between blocks, as well as the detection of possible new contacts in large displacement analysis [29]. Contact displacement increments are calculated from the relative movements of the interacting blocks. Contact forces and stresses are updated by invoking the contact constitutive equations, as described in the previous section. For the internal zones or elements, the new nodal displacements lead to the new strains, from which zone stresses ensue by applying the assumed material constitutive model. The assembled nodal forces, according to equation (8), allow the application of equation (7) for the next step.

In the present work, this dynamic algorithm is also used to obtain static solutions, by means of dynamic relaxation. In this procedure, artificial damping is applied to reach the equilibrium state. In order to improve the convergence rate, an adaptive procedure is used to continuously update the damping parameter α in equation (9) [29]. The convergence criterion is based on attaining, at all nodes, a very low value of the ratio of the nodal unbalanced force to the typical nodal force. The central difference method is only conditionally stable. To avoid numerical instabilities, a limiting time step is evaluated. In case of deformable blocks, the limiting time step is calculated, by analogy to a simple degree-of-freedom linear elastic system, for each node as:

$$\Delta t = 2 \, f_R \left(\frac{m}{K_N} \right)^{0.5}, \tag{12}$$

where m is the nodal mass, K_N is an upper-bound of the nodal stiffness, obtained by summing the stiffness of all the elements and contacts connected to the node. The user-defined factor f_R may be used to reduce the time-step [29]. The time step adopted in the analysis is the minimum value of equation (12) for all the nodes. The main disadvantage of this solution procedure is that many steps may be required to reach equilibrium, or to attain a failure mechanism. On the other hand, the small time steps typically provide a robust solution method that follows closely the nonlinear response of the contacts, including the progressive changes in contact conditions.

3 Development of the computational models for soil-structure interaction in masonry arch bridges

To demonstrate the effectiveness of the proposed computational modelling approach, this section presents the development and validation of the computational models used to investigate three different approaches to represent backfill and investigate soil-structure interaction phenomena in masonry arch bridges. Extensive information of the development of the computational models and comparisons with experimental results are presented below.

3.1 Experimental test setup

The suitability of each of the computational modelling approaches were compared to full-scale experimental tests carried out on the Prestwood Bridge, located in Staffordshire, UK. Prestwood Bridge has a span of 6.550 m and a rise of 1.428 m. The vault barrel, which is a single ring of bricks laid as headers, has a thickness of 0.220 m. The width of the bridge is 3.8 m. The backfill depth at the crown is 0.165 m. According to [34], the backfill material presents a small amount of ‘‘reddish-brown sand *with a little clay’’*. Material tests of the fill showed 7 kPa cohesion and 37° as internal frictional angle. The density of the brickwork was 2,000 kg/m^3, while the measured secant modulus of the brickwork was 4.14 GPa, (v=0.3). A line load was applied at quarter span across the width of the bridge using a 300 mm wide loading element. This was to avoid the effect of a concentrated load and premature failure of the fill. Hydraulic jacks were used to apply the load at increments until the bridge was not able to carry further load and ultimately collapsed. At each loading increment, displacements were measured remotely using total stations. The maximum load applied to the bridge before collapse was 228 kN, with the first visible evidence of damage appearing at a load of 173 kN. Failure was due to the formation of a four-hinge mechanism as shown in Figure 4. The failure mechanism was developed with minimal or negligible material crushing. Further details of the execution of the experimental test and results carried out by the Transport and Road Research Laboratory (TRRL) can be found in [34].

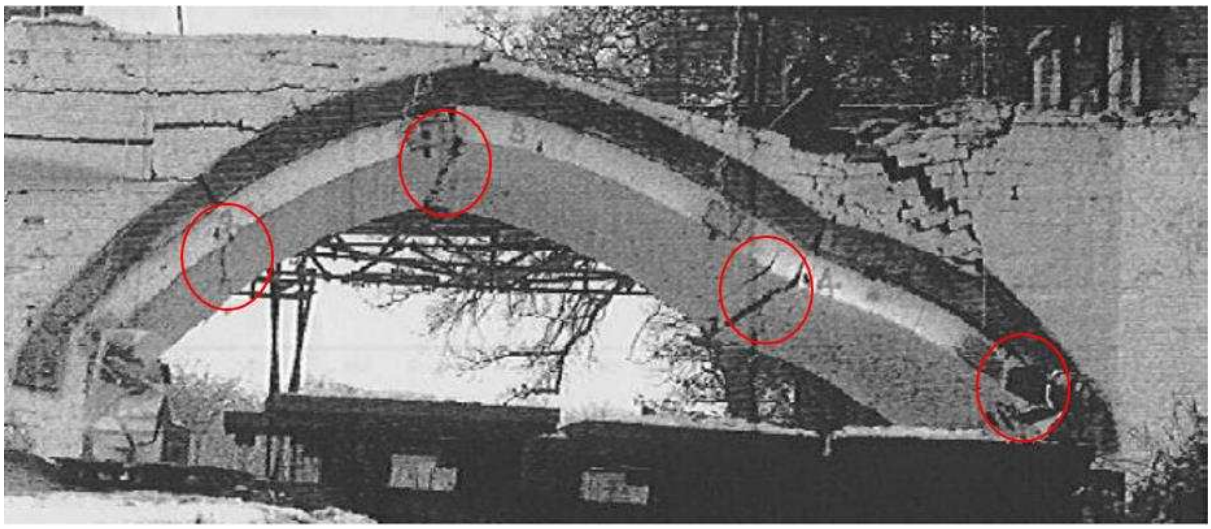

Figure 4 - Collapse mechanism of the Prestwood Bridge test (Page [34])

3.2 Development of the computational model

Geometric models to represent the geometry of the Prestwood Bridge were created in the computational model. The geometrical characteristics of the bridge were taken from [34] and can be seen in Figure 5. The numerical model contains 40 courses of voussoirs. All of the discrete elements in the model were made from linear elastic elements. Mortar joints between bricks were represented as zero thickness interface elements behaving according to the Coulomb failure criterion, which limits shear stresses along joints.

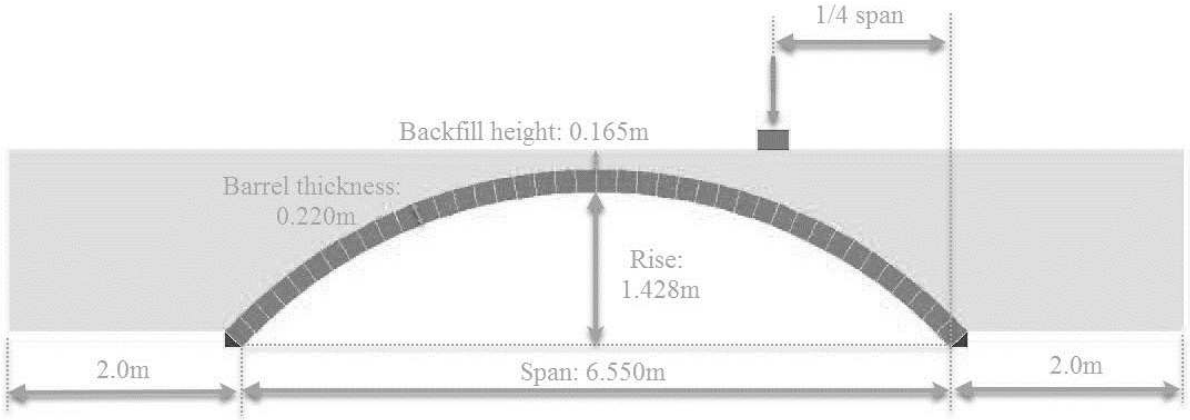

Figure 5 - Typical geometry developed using the DEM model

The material properties of the Prestwood bridge were obtained from the original experimental test report [34] and are summarized in Chapter 3.1. The Young's modulus of the discrete elements representing the voussoirs is set equal to elastic modulus of brickwork (i.e. brick and mortar). Hence, the mechanical role of the normal stiffness of the brick-brick interface element is only to avoid the interpenetration between the discrete blocks. Therefore, the normal stiffness of these interfaces is set to a sufficiently high value (see Table 1). The shear stiffness of brick-brick interface was chosen to represent the 1:2:9 mortar behaviour described in [35]. Since properties of the brick and mortar were not measured during the experiment, they were obtained from the literature, where other researchers tried to model the bridge. Thus, the friction between the bricks was set to 30°, while the cohesion and the tensile strength of the mortar was set to a low value, which can represent the behaviour of a 1:2:9 mortar. The mortar properties used for the development of the computational model are shown in Table 1.

On the extrados of the arch, a brick-to-soil interface was assigned in the numerical model. According to [36], the friction angle of the brick to soil interface depends on the roughness of the surface of the masonry units and the type of the backfill material. In the current study, material calibration undertaken and the friction angle of the brick-to-soil interface was assumed to be equal to 2/3 of the internal friction of the backfill.

Table 1 - Material properties of the interfaces

	k_n [GPa/m]	k_s [GPa/m]	φ [°]	c [MPa]	f_t [MPa]	ψ [°]
Mortar joint interface	35.0	7.0	30.0	0.05	0.05	0.0
Arch ring-backfill interface	35.0	7.0	25.0	0.00	0.00	0.0

With the aim to select the appropriate size of meshing, convergence studies were carried out. From the outcomes of the convergent studies it was found that the size of finite element mesh should be equal or less than 10 cm for the bricks and 10 cm for the backfill. The mesh assigned to the masonry arch bridge model is shown in Figure 6.

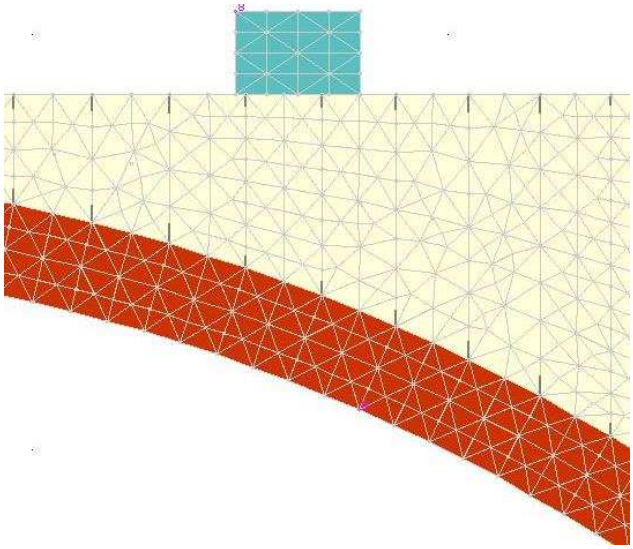

Figure 6 – Triangular finite element mesh of bricks, backfill and loading plate as obtained from the numerical model (Figure 2 shows part of the masonry arch bridge)

The developed 2D numerical model simulates plain strain conditions. Similar to the numerical model developed by Cavicchi and Gambarotta [17], the base of the masonry arch bridge, as well as the left and right hand sides of the backfill were fixed in all directions. According to these authors, the capacity of the soil due to the cohesion of the backfill should be enough to avoid plastic lateral flow of the backfill [17]. In addition, self-weight effects were assigned as gravitational load. Gravitational forces give rise to compressive forces within the voussoirs of the arch and result in its stabilisation.

Initially, the model was brought into a state of equilibrium under its own self-weight by ensuring that the maximum out-of-balance force was less than 0.001% of the total weight of the structure. Then, a constant vertical velocity equal to 0.001 m/s applied to the load spreader plate at the top of the bridge at quarter span of the arch. In order to maintain the analysis in a static manner and avoid that the structure has a dynamic response, the velocity applied to the loading element had to be closely examined and selected. To ensure a quasi-static behaviour of the masonry arch bridge, during simulations different magnitude velocities were applied in the bridge model and a converge test was carried out.

A FISH function (internal programming language of UDEC) that was able to record the reaction forces from the fixed velocity grid-points acting on the spreader plate (or platen) at each time step was written. Such conditions were selected to replicate the real conditions of the experimental loading test carried out by TRRL. Histories of displacements at the intrados of the arch have been recorded at all times (See Figure 7- coloured in red and green and marked as -4…0…4; 5).

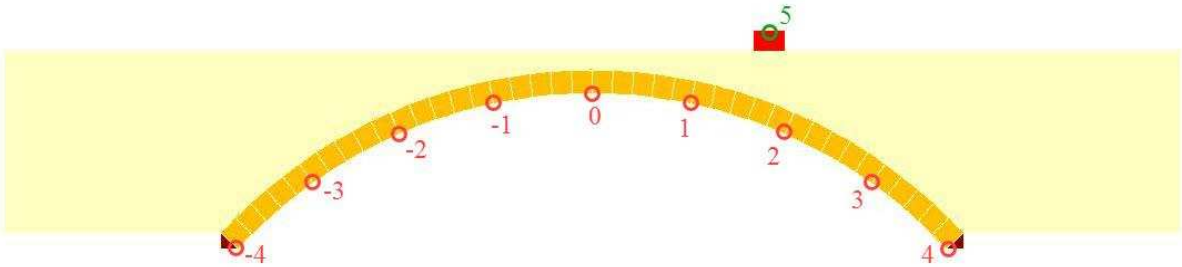

Figure 7 – Locations where vertical displacements were recorded during the numerical simulation

To model the behaviour of the backfill material, three main type of numerical models were developed and their suitability to represent the mechanical behaviour of real masonry arch bridges was investigated. In particular, the backfill of the masonry arch bridge was represented as:

(i) a single block behaving in an elasto-plastic manner;
(ii) a series of inner-backfill particles behaving in an elasto-plastic manner.
(iii) a series of inner-backfill particles behaving in an elastic manner;

For case (i) and when the backfill was represented as a single discrete block, the backfill was discretized into triangular finite element meshes. The constitutive law was allowed to represent the mechanical behaviour of the backfill material was chosen to behave according to the Mohr-Coulomb failure criteria. This approach to model the backfill is almost identical to that proposed by common models based on the finite element method (FEM). The material properties of the backfill are summarized in Table 2. Also, in the proposed model, it was assumed that crushing failure at the bricks does not occur. This is what has been observed from the experimental study as well (Page [34]).

Table 2 - Material properties of the backfill

ρ [kg/m^3]	E [GPa]	ν [-]	φ [°]	c [kPa]	f_t [kPa]
2000	0.3	0.3	37.0	7.0	7.0

An alternative approach to model the backfill of the masonry arch bridge was proposed in cases (ii) and (iii) in which the backfill material was represented as an assemblage of the so-called Voronoi-cells or inner-backfill particles. To create these cells, "seeds" were generated randomly within the boundary of the backfill domain, and for each seed, a corresponding region consisting of all points closer to that seed was determined. In this way, inner backfill particles consisting of convex elements were created. Inner-backfill particles could behave either in linear elasto-plastic (ii) or elastic (iii) manner. One of the major advantages of this approach is its potential to predict cracking in the backfill due to the application of the external load. Further details about the development of the novel approach are presented below. The numerical model which contains inner-backfill particles is shown in Figure 8.

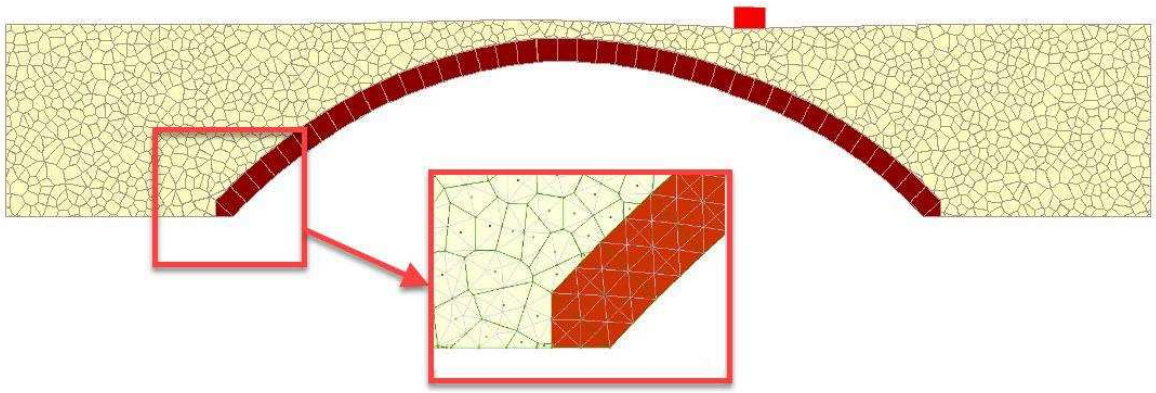

Figure 8 – Numerical model with inner-backfill particles (average inner-backfill particles element length is 10 cm).

To represent the discrete nature of the backfill, a series of irregular in shape Voronoi elements (inner-backfill particles) were introduced. These inner-backfill particles are densely packed; i.e. there is no gap between them. These particles were modelled as deformable blocks and were subdivided into triangular finite element zones. The average edge length of the finite element mesh assigned in each inner-soil element was 10 cm (independently from the size of the inner-backfill particles). In the numerical model, inner-backfill particles were separated by a zero-thickness interface. Such interfaces possess finite stiffness, which means, if the number of Voronoi-cells increases (i.e. the size of the inner-backfill particles is decreasing) the structural behaviour will be softer. To avoid this effect, the stiffness

of these interfaces was chosen inversely proportional to the average size of the Voronoi-cells (v_l). In the case of the elasto-plastic inner-backfill particles, the elastic properties of the backfill were incorporated into the elastic material properties, hence the role of the interface's normal stiffness is to avoid the interpenetration of the elements. In the case (iii), the inner-backfill particles simulated as linear elastic, isotropic material while their interaction with each other was controlled by Coulomb friction law. In this situation, the plastic behaviour of the backfill was incorporated into the interface elements between the inner-backfill particles. The internal friction angle, the cohesion and the tensile strength of these interfaces were chosen according to Table 4. In the case of purely elastic inner backfill elements, the stiffness of interfaces has to be decreased in order to avoid interlocking of the densely packed Voronoi-cells. A calibration procedure is presented below. The material properties for the interfaces of the inner-backfill particles are summarized in Table 3. In the model, the zoning properties, boundary conditions and loading remained unchanged to before.

Table 3 - Properties of interfaces between Voronoi-cells (or inner-backfill particles)

	k_n [Pa/m]	k_s [Pa/m]	φ [°]	c [kPa]	f_t [kPa]	ψ [°]
Interfaces between elasto-plastic Voronoi-cells	$\frac{200\text{MPa}}{v_l}$	$\frac{100\text{MPa}}{v_l}$	37.0	7.0	7.0	0.0
Interfaces between linear elastic Voronoi cells	$\frac{20\text{MPa}}{v_l}$	$\frac{10\text{MPa}}{v_l}$	37.0	7.0	7.0	0.0

4 Results and Discussion

4.1 Backfill as a single elasto-plastic block

The load against quarter-span displacement relationship obtained from the numerical model was compared to the maximum load carrying capacity of the masonry arch bridge obtained from the experiment (Figure 9). The experimental collapse load of the Prestwood Bridge was 228 kN (Page [34]), while the ultimate load bearing capacity obtained from this discrete element numerical model using UDEC was 219 kN. From the above, the error percentage for the maximum load from the numerical model against the experimental result is 4%.

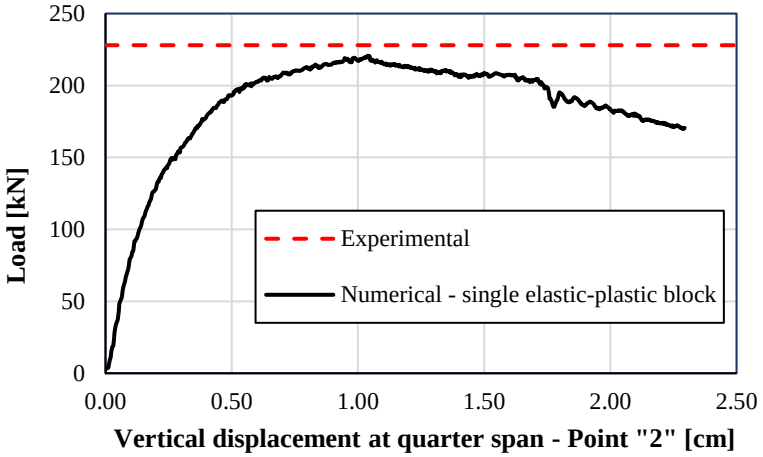

Figure 9 - Load-displacement curve. Backfill represented by a single elastic-plastic block model

Verification on the suitability of the numerical model to capture the failure mode has also been undertaken. The collapse mechanism obtained from the numerical model was compared to the failure mechanism observed during the experiment. From Figure 10b, the four-hinge mechanism in the arch ring is evident. Moreover, it is appreciated how the backfill under the applied load moved downwards,

while the backfill to the left side of the bridge moved upwards i.e. the typical sway mechanism. Slight difference can be found at the second hinge position. It should be noted, that the left abutment of the bridge was 8 cm higher compared to the right one. This imperfection can cause small differences in the failure mechanism.

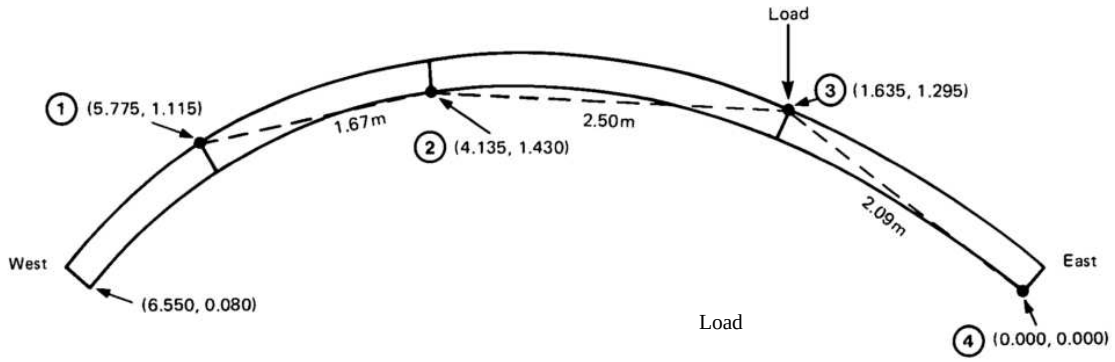

(a)

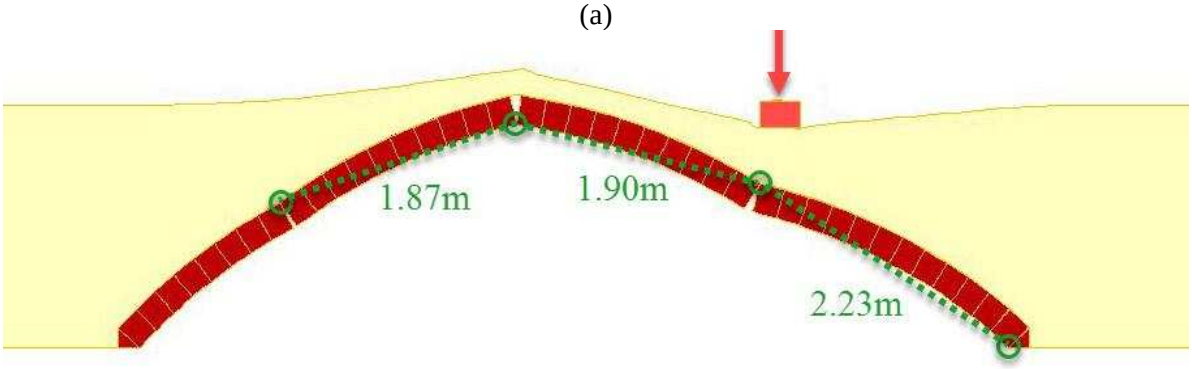

(b)

Figure 10 – Failure mechanisms: (a) experiment; (b) numerical simulation

The thrust line within the arch barrel can be observed with the help of principal stress trajectories (see Figure 11). In the location of plastic hinges, the adjacent voussoirs contacted with each other on a very narrow surface able to cause stress concentrations within the elements.

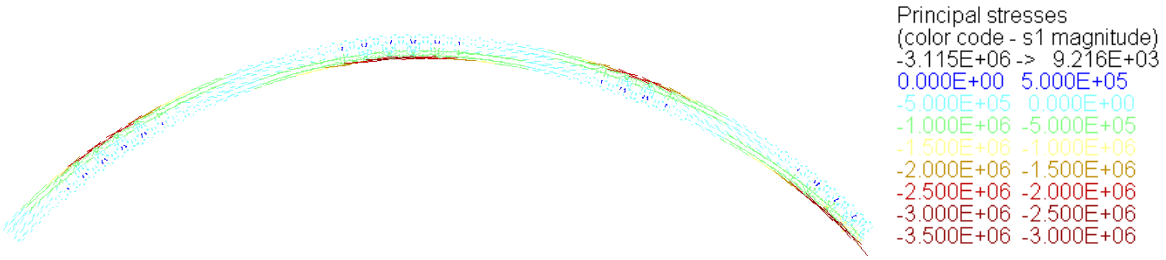

Figure 11 – Principal stress trajectories in the arch barrel

The stresses and the plastic state of the backfill was measured during the numerical simulation and can be seen in Figure 12. Initially, the external load is negligible compared to the self-weight of the structure. Therefore, the contour of compressive principal stresses is nearly symmetric (Figure 12b). As the intensity of the external load is increasing at quarter span, firstly, the active earth pressure was activated below the loading element and later, with the application of further external load on some passive earth pressure was mobilized at the left part of the structure (Figure 12d, e, f).

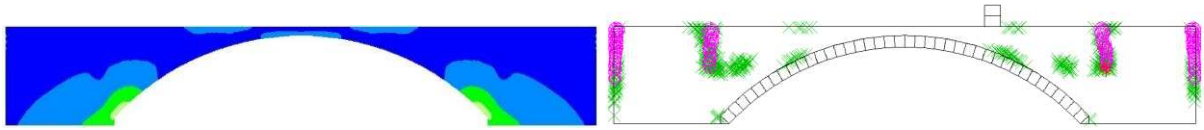

a.) Self-weight

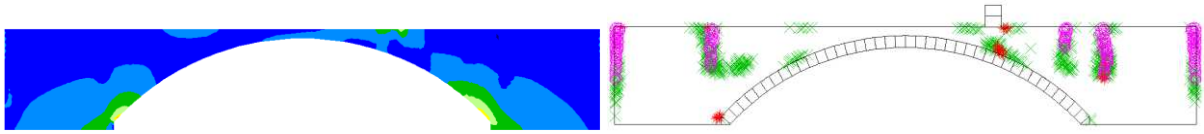

b.) 40 kN

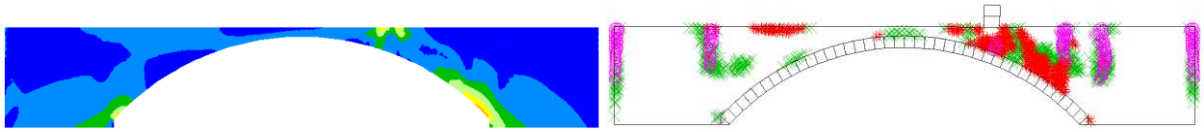

c.) 90 kN

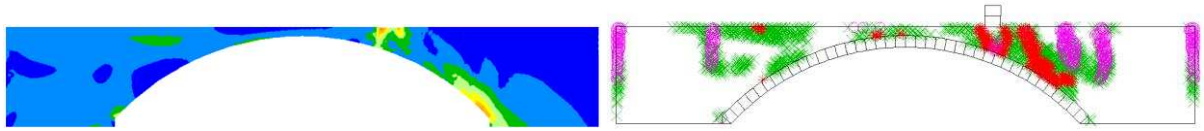

d.) 130 kN

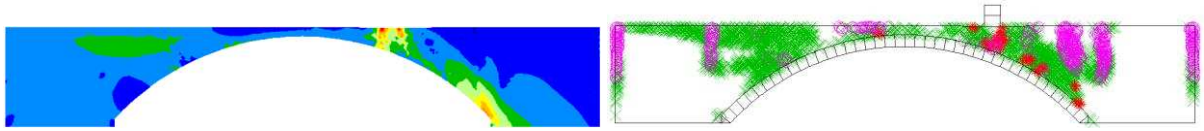

e.) 170 kN

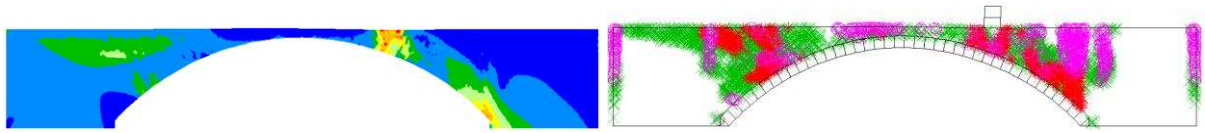

f.) Failure load: 216 kN

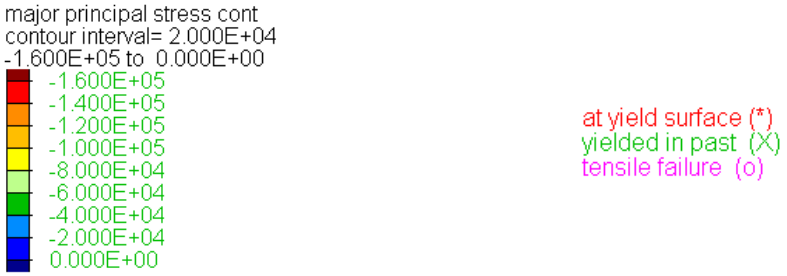

Figure 12 - Failure mechanism of the masonry arch bridge as obtained from the numerical model – Backfill simulated as a single elastic-plastic block

4.2 Backfill represented as inner-backfill particles (or Voronoi-cells)

In the following section, the results of the alternative approach to simulate backfill materials are presented. The effect of different Voronoi-sizes and interface stiffnesses on the mechanical behaviour is discussed. The forthcoming questions are addressed in this section:

- How the adequate average Voronoi-cell size should be chosen to ensure accurate estimation of the load bearing capacity of the arch bridge?
- What is the mechanical role of the inner backfill interfaces and how to choose their contact stiffnesses?

To answer the first question, masonry arch bridges having different in size Voronoi-cells to represent the backfill material were investigated. The size of the Voronoi-cell sizes ranged from 0.05m to 0.75m (see Figure 13). To answer the second question, various bridge models were undertaken in which Voronoi cells were allowed to behave according to: a) an elasto-plastic; and b) elastic manner. Results and discussion of the simulations undertaken are presented below.

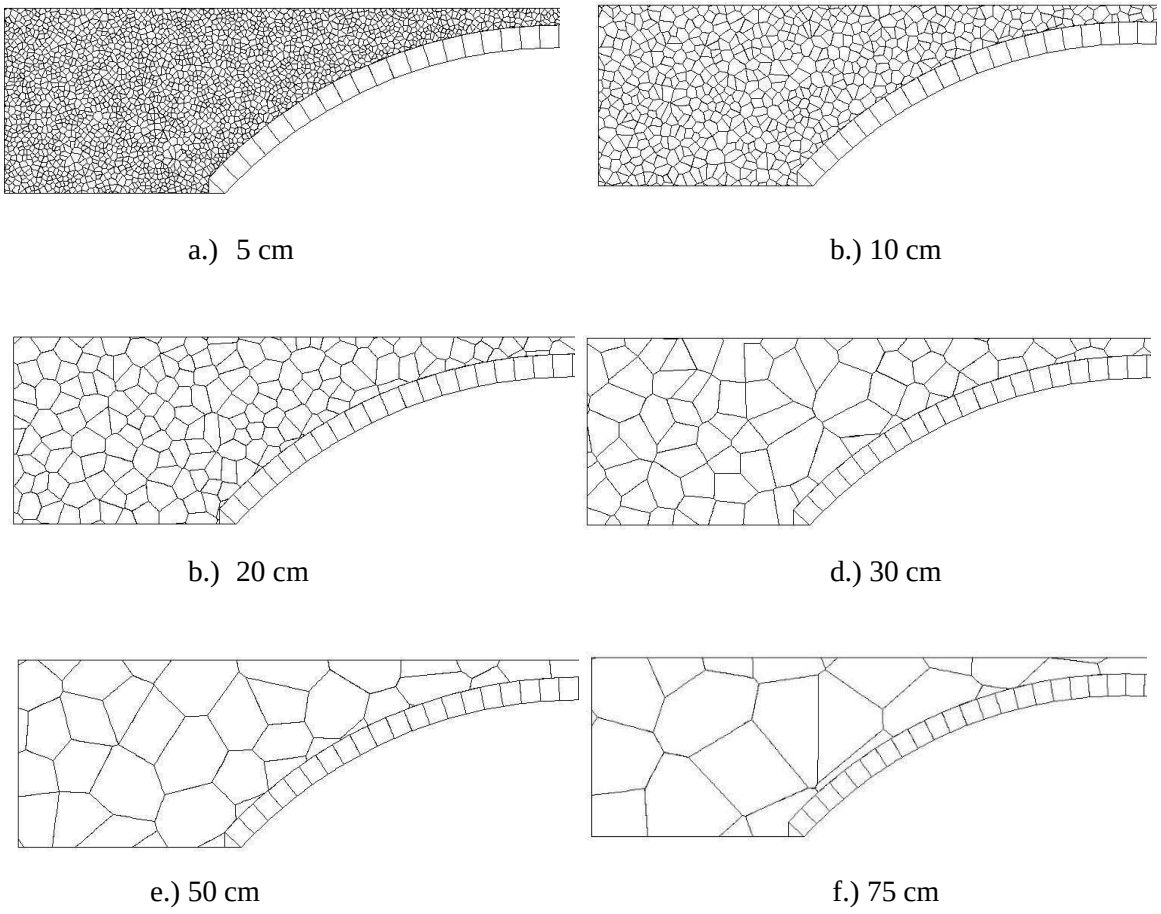

Figure 13 – Numerical models with different Voronoi cell sizes

4.2.1 Backfill represented as Voronoi-cells with elasto-plastic behaviour

In case of elasto-plastic inner-backfill particles, the ultimate load bearing capacity was not affected by the size of the Voronoi-cells (Figure 14). Plastic deformations can occur within the Voronoi cells, so even for the case of larger Voronoi cells the load bearing capacity does not vary significantly. The stiffness of the model was found to be lower when compared to the bridge model with the backfill represented by a single elasto-plastic element. This is because the bridge model with backfill as a series of Voronoi elements contains additional interfaces between the inner-backfill particles, which possess finite stiffness. Considering different Voronoi-cell sizes, there are no differences between the stiffness

either, because the applied inner-backfill interface stiffness is inversely proportional to the Voronoi size. The load bearing capacity of this model was approximately 10% lower compared to the experimental results, and ~7% lower compared to the single elasto-plastic model. The difference between the two numerical approaches can be explained as follows. In the case of the single block model, after a finite element reaches the failure surface of the Mohr-Coulomb criteria, the cohesion and the tensile strength does not drop to zero. The residual value of these strength parameters is equal to the original value, while in case of Voronoi model, after an interface is slipped or cracked, the cohesion and the tensile strength of that surfaces are set to zero.

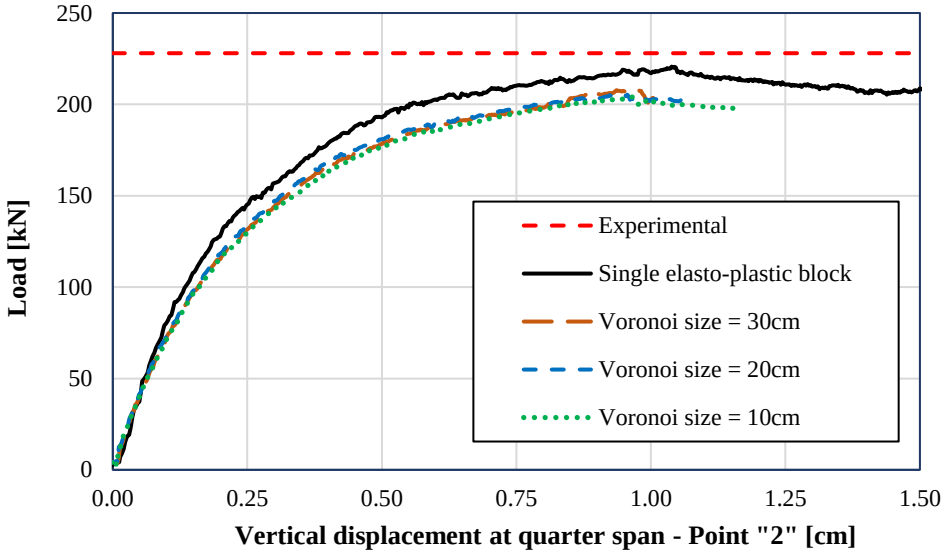

Figure 14 – Load-displacement curves for elasto-plastic Voronoi models

Although both numerical approaches (i.e. Voronoi vs single e-p block) can capture the experimental ultimate load capacity, the superiority of the approach is the fact that initiation and propagation of cracking can be obtained. In particular, regarding the failure mechanism (Figure 15), the masonry arch with elasto-plastic Voronoi backfill model failed by a four-hinge mechanism. The location of hinge positions matches exactly with the model, which contains a single elasto-plastic block as backfill (Figure 10b). The biggest tensile crack was developed almost vertically above the right abutment. Smaller tensile cracks appeared below the loading element, above the crown. There were some slipped Voronoi elements in the vicinity of the passive earth pressure.

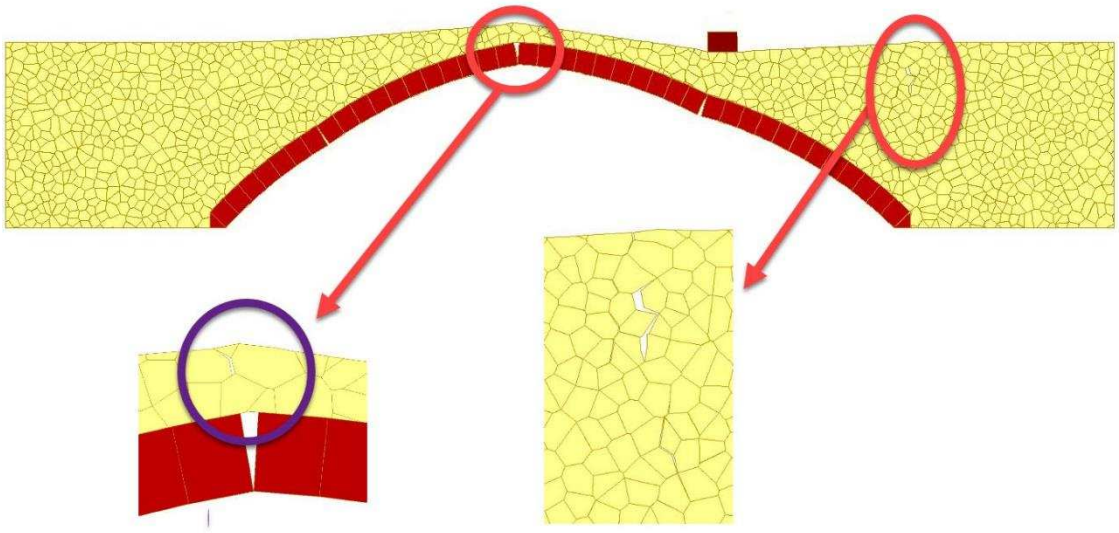

Figure 15 – Failure mechanism of elasto-plastic Voronoi model (average element length is 10 cm)

4.2.2 Backfill represented as Voronoi-cells with elastic behaviour

The following results are connected to the numerical models, which contain elastic Voronoi cells, which represent the inner backfill particles. In these models, the plastic behaviour of the backfill was incorporated into the inter-backfill interfaces.

Firstly, the stiffness of the inner backfill interfaces was calibrated. In Figure 16, load displacements curves of the numerical model with a fixed, 10 cm Voronoi cells are presented. With the increasing contact stiffness, both stiffness and load bearing capacity of the structure are increasing. In case of lower stiffness, the interpenetration of the Voronoi cells is larger, which enables the development of the failure mechanism. In case of high contact stiffnesses interlocking between the Voronoi cells occurs, which numerically increases the load bearing capacity of the structure. The contact stiffness depends on the chosen tessellation, on the shape of the elements. In addition, from Figure 16, it is evident that for all arche bridge models investigated, the maximum load that the arch can carry was observed when the quarter span displacement was around 1.5 to 2 cm.

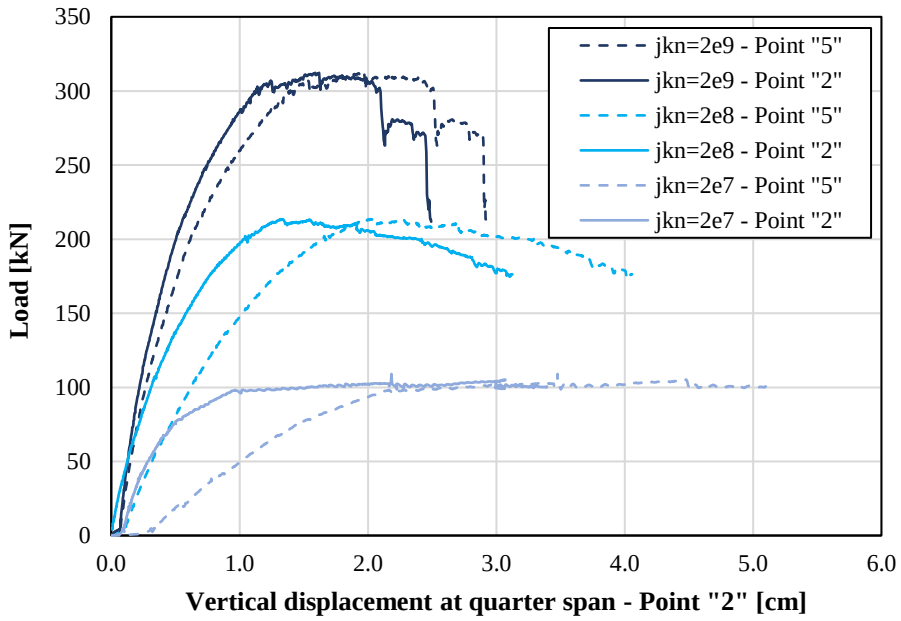

Figure 16 – Load-displacement curves of elastic Voronoi model with different inner-backfill interface stiffness, k_n [N/m^3] (average cell size: 10 cm)

The effect of the size of the Voronoi elements (or inner soil particles) was investigated in Figure 17. From Figure 17, as the average size of the Voronoi elements decreases, the ultimate load bearing capacity of the structure converges to a constant value, which in this case is close to the ultimate load carrying capacity obtained from the experimental study. Also, the smaller the size of the Voronoi, the less stiff the masonry arch bridge.

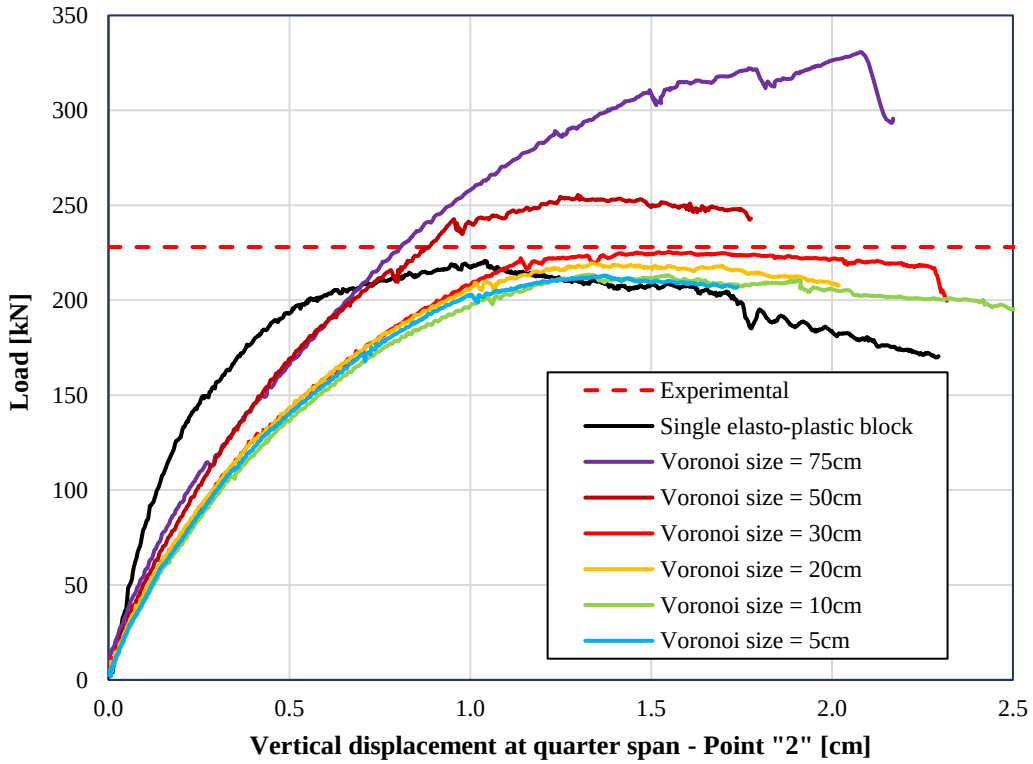

Figure 17 -Load displacement curves of elastic Voronoi model, with different size of Voronoi elements

Figure 18 compares the ultimate load against the average size of the inner backfill particle (or Voronoi element). According to Figure 18, the difference between the load bearing capacity of the 5cm and 30cm model was around 6%. Considering the average size of the numerical model (~8m x 2m), it is suggested that the applied Voronoi cell size should be less than the 3% of the greatest model dimension.

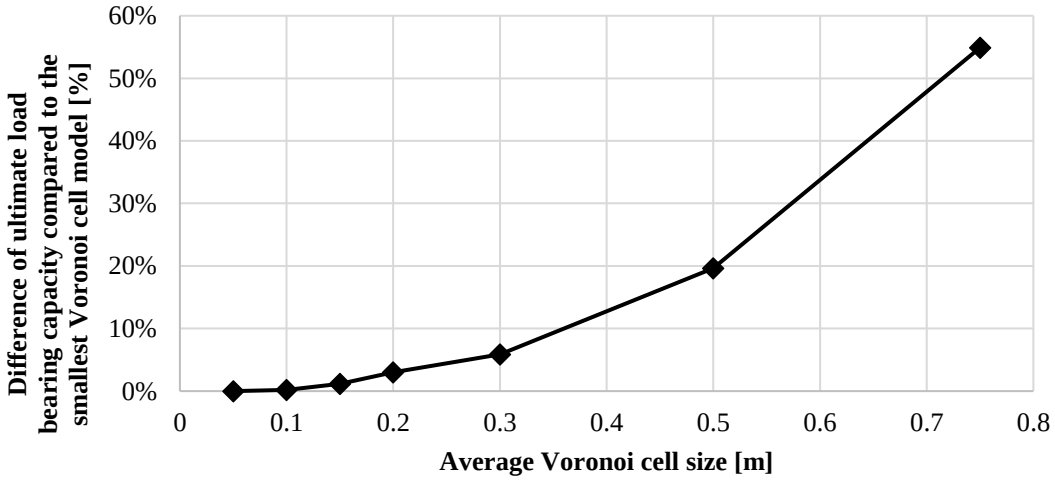

Figure 18 – Convergence of the ultimate load in case of different Voronoi cell size

Compared to the elasto-plastic Voronoi case, the size and the number of cracks was bigger. During the loading procedure, in order to develop the failure mechanism within the backfill, the densely packed Voronoi cells needed to separate or slide upon each other. Thus, the deformation of the backfill appeared in the form of cracks, and sliding movements. In Figure 19, the crack propagation can be seen in the case of 5 cm Voronoi cells. The biggest crack appeared above the right abutment, similarly to the elasto-plastic Voronoi cells (Figure 15).

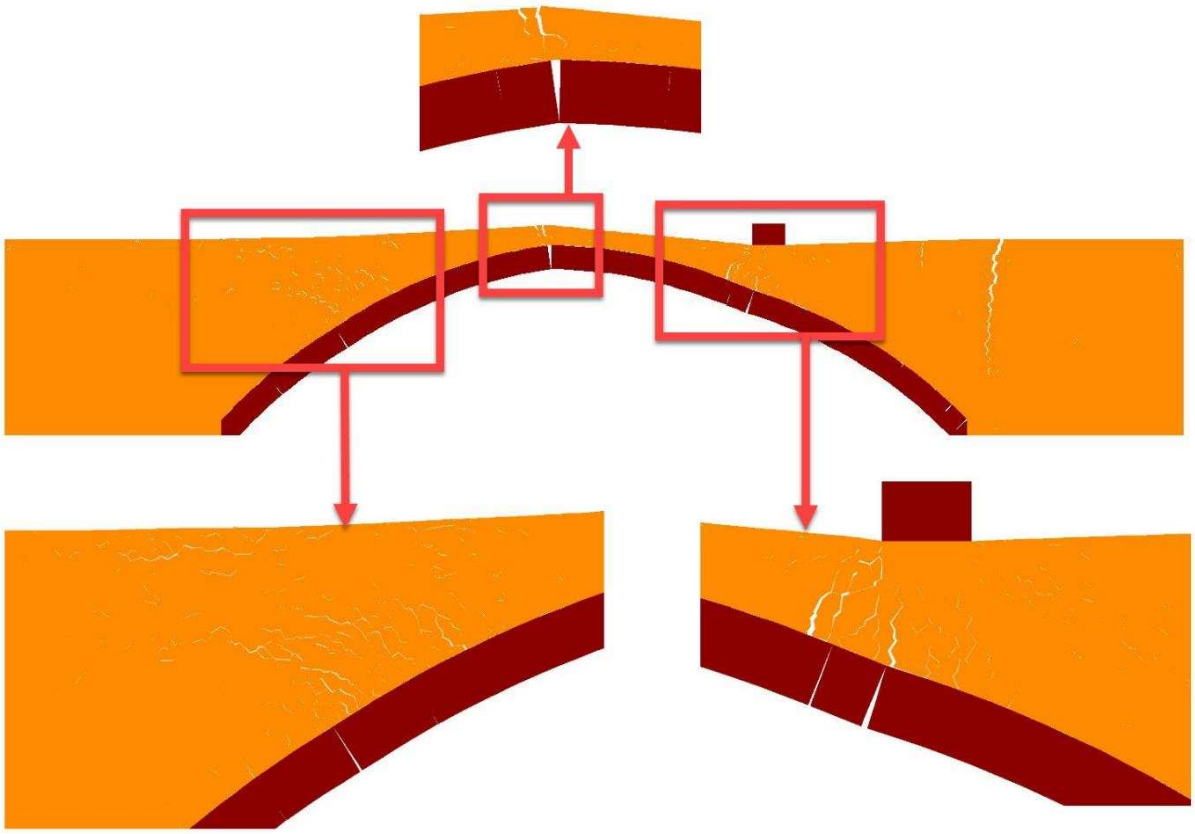

584

585 **Figure 19** – Crack propagation within the soil – average Voronoi-cell size: 5 cm.

586 Figure 20 shows the vertical displacements at ultimate load bearing capacity along the length of the
587 arch barrel for the different models developed (note point ID 2 is where the load applied, see also Figure
588 7). From Figure 20, the displacements are the same for the model in which backfill was considered as
589 a single elastic-plastic block as well as for the model where the backfill is considered as a series of
590 Voronoi elements behaving in an elastic-plastic manner. On the contrary, for the model in which backfill
591 was represented as a series of Voronoi elements behaving in an elastic manner, the displacements are
592 higher. This may be due to the interfaces between inner-backfill particles, which can move and rotate
593 freely as well as due to the hinging mechanism of the backfill particles.

594

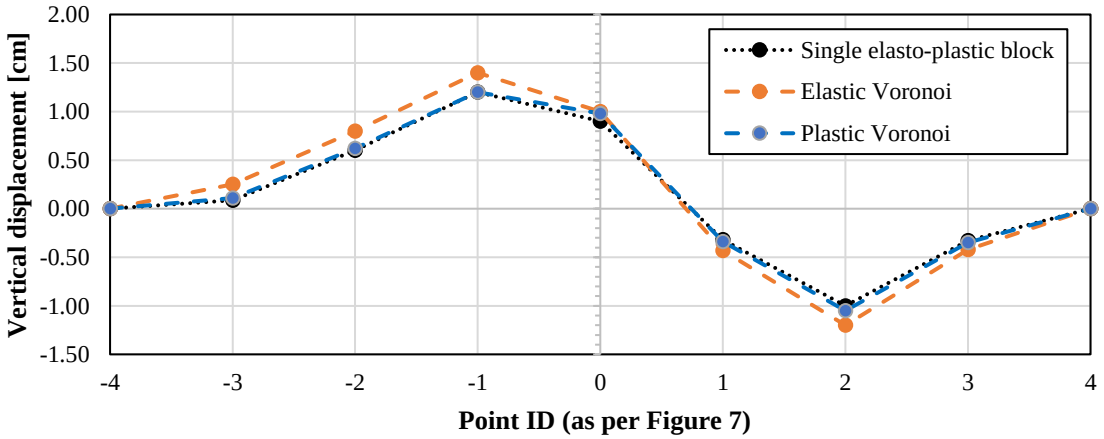

595

596 **Figure 20** – Vertical displacements of the arch barrel for the different ID points shown in Figure 7

5 Conclusions

Many masonry arch bridges still in service are relatively old but subject to increasing vehicle loads. Past research demonstrated that load-carrying capacity of a masonry arch bridge is significantly affected not only by the backfill material, but also by the backfill to arch ring interaction. These interaction phenomena are not taken into account by many over-simplified approaches commonly used.

A novel modelling approach for the simulation of backfill in masonry arch bridges, based on the discrete element method, has been proposed. Bricks in the barrel vault are represented as an assembly of distinct blocks separated by zero thickness interfaces at each mortar joint, while backfill is represented as an assemblage of densely packed discrete irregular deformable particles. The mechanical behaviour of the backfill is influenced by the size and properties of the irregular soil particles and contacts. A series of computational models were developed, and their results compared against full-scale experimental results. A good agreement between the experimental and the numerical results was obtained demonstrating the significant potential of the proposed approach. The major findings of the proposed approach are summarized below:

- The four-hinge failure mechanism obtained with the three numerical models developed (the single block elasto-plastic soil, the elastic Voronoi, and the elasto-plastic Voronoi) is in good agreement with the experimental failure mode.
- The Voronoi models have the advantage of naturally modelling crack initiation and propagation as real discontinuity between soil particles. In particular, failure surfaces developing from the extrados hinges into the soil can be clearly represented. The randomness of the Voronoi patterns minimizes the possible mesh effects on fill behaviour.
- The three computational models developed herein were able to provide a good approximation of the experimental failure load. However, in the model with elastic Voronoi, the ultimate load bearing capacity was influenced by the properties (and in particular the stiffness properties) of the soil-to-soil particles, which have to be calibrated. Therefore, the elasto-plastic Voronoi model appears more robust.
- Crack location and propagation in the backfill and the overall structure is more accurate for smaller size Voronoi elements. Larger size Voronoi elements lead to higher load carrying capacity of the bridge, but failure mode remains a four-hinge mechanism.

Although the authors understand that arch and the backfill system constitute a 3D domain having finite thickness, the present work aims at assessing the suitability of the Voronoi/inner soil particles model, which is more efficiently performed using two dimensional models. Also, as part of this study, the effect of the spandrel is ignored, since it is impossible to model them in a 2D model (plane strain). In the future, further research is going to be carried to include the three-dimensional effects of the Voronoi particles as well as investigate methodologies used for the calibration of the interface material properties between inner soil elements and how such micro-parameters affect the global behaviour of the bridge. In addition, the suitability of the approach to masonry arch bridges subjected to geometric irregularities as well as mechanical behaviour under earthquake load conditions will be evaluated.

Acknowledgement

The work presented in this paper was partially financially supported by an EPRSC doctoral training award (CASE/179/65/82).

References

[1] Davey N. Tests on road bridges: HM Stationery Office; 1953.
[2] Harvey W, Vardy A, Craig R, Smith F. Load tests on a full scale model four metre span masonry arch bridge. 1989.
[3] Melbourne C. Conservation of masonry arch bridges. Brick and Block Masonry. 1991;3:1563-70.
[4] Gilbert M. The behaviour of masonry arch bridges containing defects: University of Manchester; 1993.

[5] Melbourne C, Walker P. Load test to collapse on a full scale model six metre span brick arch bridge. 1990.
[6] Fairfield C, Ponniah D. MODEL TESTS TO DETERMINE THE EFFECT OF FILL ON BURIED ARCHES. P I Civil Eng-Str B. 1994;104:471-82.
[7] Hughes T, Davies M, Taunton P. The influence of soil and masonry type on the strength of masonry arch bridges. Arch Bridges History, analysis, assessment, maintenance and repair. 1998:321-30.
[8] Gilbert M, Smith C, Melbourne C, Wang J. An experimental study of soil-arch interaction in masonry bridges2006.
[9] Melbourne C, Gilbert M. The behaviour of multi-ring brickwork arch bridges containing ring separation. Proceedings of the 3rd International Conference of the British Masonry Society1992. p. 218-24.
[10] Forgacs T, Sarhosis V, Ádány S. Discrete Element Modeling of skew masonry arch bridges taking into account arch ring-backfill interaction. In: Milani G, Taliercio A, Garrity S, editors. 10th International Masonry Conference. Milan, Italy2018.
[11] Lourenco PB. Computational modelling of masonry structures: Delft University of Technology; 1996.
[12] Boothby TE. Analysis of masonry arches and vaults. Progress in Structural Engineering and materials. 2001;3:246-56.
[13] Callaway P, Gilbert M, Smith CC. Influence of backfill on the capacity of masonry arch bridges. Proceedings of the Institution of Civil Engineers: Bridge Engineering: ICE Publishing; 2012. p. 147-57.
[14] Gilbert M, Ahmed HM. Developments to the RING masonry arch bridge analysis software. P Roca and C Molins, Fourth International Conference on Arch Bridges, Barcelona2004. p. 263-72.
[15] Gilbert M, Casapulla C, Ahmed HM. Limit analysis of masonry block structures with non-associative frictional joints using linear programming. Comput Struct. 2006;84:873-87.
[16] Gilbert M, Smith CC, Hawksbee SJ, Melbourne C. Modelling Soilstructure interaction in masonry arch bridges. 7th International Conference on Arch Bridges, In: Radiae J, Kuster M, Savor Z2013. p. 613-20.
[17] Cavicchi A, Gambarotta L. Lower bound limit analysis of masonry bridges including arch–fill interaction. Engineering Structures. 2007;29:3002-14.
[18] Zhang YY, Macorini L, Izzuddin BA. Numerical investigation of arches in brick-masonry bridges. Structure and Infrastructure Engineering. 2018;14:14-32.
[19] Zhang Y, Tubaldi E, Macorini L, Izzuddin BA. Mesoscale partitioned modelling of masonry bridges allowing for arch-backfill interaction. Constr Build Mater. 2018;173:820-42.
[20] Milani G, Lourenco PB. 3D non-linear behavior of masonry arch bridges. Comput Struct. 2012;110:133-50.
[21] Forgács T, Sarhosis V, Bagi K. Influence of construction method on the load bearing capacity of skew masonry arches. Engineering Structures. 2018;168:612-27.
[22] Sarhosis V, Oliveira DV, Lemos JV, Lourenco PB. The effect of skew angle on the mechanical behaviour of masonry arches. Mech Res Commun. 2014;61:53-9.
[23] Forgacs T, Sarhosis V, Bagi K. Minimum thickness of semi-circular skewed masonry arches. Engineering Structures. 2017;140:317-36.
[24] Sarhosis V, De Santis S, de Felice G. A review of experimental investigations and assessment methods for masonry arch bridges. Structure and Infrastructure Engineering. 2016;12:1439-64.
[25] De Santis S, de Felice G. Overview of railway masonry bridges with a safety factor estimate. International journal of architectural heritage. 2014;8:452-74.
[26] Thavalingam A, Bicanic N, Robinson J, Ponniah D. Computational framework for discontinuous modelling of masonry arch bridges. Comput Struct. 2001;79:1821-30.
[27] Fang Y-S, Ho Y-C, Chen T-J. Passive earth pressure with critical state concept. Journal of Geotechnical and Geoenvironmental Engineering. 2002;128:651-9.
[28] Cundall PA. A computer model for simulating progressive, large-scale movements in blocky rock systems. Proc Int Symp on Rock Fracture. 1971:11-8.
[29] ITASCA. UDEC - Universal Distinct Element Code Manual. Theory and Background. Mineapolis, USA: Itasca Consulting Group; 2004.

[30] Mayya N, Rajan V. An efficient shape representation scheme using Voronoi skeletons. Pattern Recognition Letters. 1995;16:147-60.
[31] Lemos JV. Discrete Element Modeling of Masonry Structures. International Journal of Architectural Heritage. 2007;1:190-213.
[32] Sarhosis V, Garrity S, Sheng Y. A computational modelling approach for low bond strength masonry. 2012.
[33] Hughes TJ. The finite element method: linear static and dynamic finite element analysis: Courier Corporation; 2012.
[34] Page J. Load tests to collapse on two arch bridges at Preston, Shropshire and Prestwood, Staffordshire. 1987.
[35] Van der Pluijm R. Out-of-plane bending of masonry: behaviour and strength. 1999.
[36] Jensen JS, Casas JR, Karoumi R, Plos M, Cremona C, Melbourne C. Guideline for load and resistance assessment of existing european railway bridges. Fourth International Conference on Bridge Maintenance, Safety and Management (IABMAS 08). France2008. p. pp 3658-65.
[37] Zampieri P, Cavalagli N, Gusella V, Pellegrino C. Collapse displacements of masonry arch with geometrical uncertainties on spreading supports, Computers & Structures, 2018; 208:118-129.